

**Separating Geophysical Signals Using GRACE and High-Resolution Data  
A Case Study in Antarctica**

Engels, Olga; Gunter, Brian; Riva, Riccardo; Klees, Roland

**DOI**

[10.1029/2018GL079670](https://doi.org/10.1029/2018GL079670)

**Publication date**

2018

**Document Version**

Final published version

**Published in**

Geophysical Research Letters

**Citation (APA)**

Engels, O., Gunter, B., Riva, R., & Klees, R. (2018). Separating Geophysical Signals Using GRACE and High-Resolution Data: A Case Study in Antarctica. *Geophysical Research Letters*, 45(22), 12340-12349. <https://doi.org/10.1029/2018GL079670>

**Important note**

To cite this publication, please use the final published version (if applicable).  
Please check the document version above.

**Copyright**

Other than for strictly personal use, it is not permitted to download, forward or distribute the text or part of it, without the consent of the author(s) and/or copyright holder(s), unless the work is under an open content license such as Creative Commons.

**Takedown policy**

Please contact us and provide details if you believe this document breaches copyrights.  
We will remove access to the work immediately and investigate your claim.



## RESEARCH LETTER

10.1029/2018GL079670

### Key Points:

- The described approach allows data that feature high spatial resolution to be consistently combined and/or compared with GRACE data
- The described method separates the derived GIA and ice-mass change signals in Antarctica using GRACE, ICESat, RACMO, and GPS data
- The data-driven approach allows, for the first time, to retrieve the complex spatial pattern of present-day GIA in West Antarctica

### Supporting Information:

- Supporting Information S1

### Correspondence to:

O. Engels,  
engels@geod.uni-bonn.de

### Citation:

Engels, O., Gunter, B. C., Riva, R. E. M., & Klees, R. (2018). Separating geophysical signals using GRACE and high-resolution data: A case study in Antarctica. *Geophysical Research Letters*, 45, 12,340–12,349.  
<https://doi.org/10.1029/2018GL079670>

Received 20 JUL 2018

Accepted 11 NOV 2018

Accepted article online 14 NOV 2018

Published online 23 NOV 2018

Corrected 4 JAN 2019

This article was corrected on 4 JAN 2019. See the end of the full text for details.

## Separating Geophysical Signals Using GRACE and High-Resolution Data: A Case Study in Antarctica

Olga Engels<sup>1,2</sup> , Brian Gunter<sup>3</sup> , Riccardo Riva<sup>2</sup> , and Roland Klees<sup>2</sup> 

<sup>1</sup>Institute for Geodesy and Geoinformation, University of Bonn, Bonn, Germany, <sup>2</sup>Department of Geoscience and Remote Sensing, Delft University of Technology, Delft, The Netherlands, <sup>3</sup>Daniel Guggenheim School of Aerospace Engineering, Georgia Institute of Technology, Atlanta, GA, USA

**Abstract** To fully exploit data from the Gravity Recovery and Climate Experiment (GRACE), we separate geophysical signals observed by GRACE in Antarctica by deriving high-spatial resolution maps for present-day glacial isostatic adjustment (GIA) and ice-mass changes with the least possible noise level. For this, we simultaneously (i) improve the postprocessing of gravity data and (ii) consistently combine them with high-resolution data from Ice Cloud and land Elevation Satellite altimeter (ICESat) and Regional Atmospheric Climate Model 2.3 (RACMO). We use GPS observations to discriminate between various candidate spatial patterns of vertical motions caused by GIA. The ICESat-RACMO combination determines the spatial resolution of estimated ice-mass changes. The results suggest the capability of the developed approach to retrieve the complex spatial pattern of present-day GIA, such as a pronounced subsidence in the proximity of the Kamb Ice Stream and pronounced uplift in the Amundsen Sea Sector.

**Plain Language Summary** The Gravity Recovery and Climate Experiment (GRACE) satellite mission has become an indispensable tool in monitoring global mass variations. However, the limited horizontal and lacking vertical resolution of the gravity satellite data is still a major challenge. We develop an approach that allows gravity satellite data to be consistently combined with other complementary data that feature higher spatial resolution (e.g., altimetry and climate data). The consistent combination in terms of horizontal resolution allows the different signals contributing to the total GRACE signal to be accurately separated. We demonstrate the utility of the developed approach by separating present-day ice-mass changes and glacial isostatic adjustment (GIA) in Antarctica using gravimetry, altimetry, climate, and GPS data. For the first time, our data-driven approach allows the statistically significant small-scale GIA features to be retrieved, such as a pronounced subsidence in the proximity of the Kamb Ice Stream. The estimated GIA is important to validate geophysical GIA models, while accurately estimated Antarctic ice-mass changes are important for sea-level projections. Moreover, the developed method can be applied on data derived from, for example, the upcoming satellite altimetry and gravity missions and in any other application which involves GRACE data and any other geodetic data.

## 1. Introduction

The Gravity Recovery and Climate Experiment (GRACE) satellite mission has become an indispensable tool in monitoring global mass variations (e.g., Humphrey et al., 2017). However, the limited horizontal and lacking vertical resolution of the gravity satellite data still represents a major challenge. The GRACE Follow-On mission (launched in Spring 2018) is expected to exhibit similar limitations, emphasizing the need for developing robust tools to improve them.

The limited horizontal resolution is a result of (i) truncating the spherical harmonic (SH) coefficients during the processing of GRACE solutions and (ii) attempts to separate noise from signal during the postprocessing step. Noise in GRACE data (so-called *stripes*) is caused by the mission geometry in connection with limitations of current data processing strategies, instrument errors, and uncertainties in background models (Teixeira Encarnação, 2015). Filtering and/or *destriping* is the usual approach for suppressing noise in GRACE data when evaluating SHs as suggested by, for example, Wahr et al. (1998). Different filtering techniques have been

developed ranging from a simple isotropic Gaussian filter proposed by Swenson and Wahr (2006) to more sophisticated anisotropic filters (e.g., Klees et al., 2008; Kusche, 2007). However, filtering causes spatial leakage and, in turn, attenuation of signal and reduction of spatial resolution (Siemes et al., 2013). Spatial leakage prevents GRACE data from being fully exploited as it introduces an artificial redistribution of mass signal.

There have been several studies aiming at an accurate spatial localization of mass changes. Chen et al. (2015) used a forward modeling algorithm to reduce leakage between land and ocean due to the limited range of SHs and commonly used Gaussian filtering. Using synthetic data for West Antarctica (WA), they demonstrated effectiveness of restricting signal to predefined regions but did not examine whether this algorithm can cope with leakage between adjacent basins containing strong positive with neighboring negative signal, as it applies for WA. An alternative to the SH representation of surface mass changes are mascons (i.e., single layer densities), which represents an approach designed to reduce leakage and therefore increases signal recovery. The mascon basis functions are directly related to GRACE level 1B tracking data and are represented by a truncated SH expansion (e.g., Luthcke et al., 2013) or by an analytical expression (e.g., Watkins et al., 2015). As mascon shapes (discs) are not based on geophysical boundaries, they are still subject to leakage, especially near coastal regions (Watkins et al., 2015). Moreover, leakage may also occur between adjacent mascons due to the use of signal covariances that contain constraints regarding characteristic length and time (e.g., Luthcke et al., 2013). To obtain high-resolution spatial mass variation patterns while avoiding filtering of GRACE data, Baur and Sneeuw (2011) related gravity observations at the satellite altitude to point-mass variations on Earth's surface, interpreting each point as a small drainage basin. Among all parameterizations used (point masses, SHs, and mascons), the parameterization of the real time-varying gravity field by single layer densities is the closest to the physical processes causing mass changes (e.g., Ran et al., 2017; Wong et al., 1971).

Although GRACE observations directly provide mass changes, they represent a sum of signals originating from different sources. Separating geophysical signals observed by GRACE is usually performed using models or complementary data (e.g., Martín-Español, King, et al., 2016). For example, for Antarctica, present-day ice-mass changes (IMC) and glacial isostatic adjustment (GIA) are the main sources contributing to the total GRACE signal. GIA which in this study is understood as any viscoelastic response of the solid earth to changing ice loads and should be removed from GRACE observations as accurately as possible prior to deriving IMC. Unfortunately, the spatial distribution as well as the magnitude of the GIA signal are still poorly known, representing the largest source of uncertainty for Antarctic IMC estimates derived from GRACE (Sasgen et al., 2017). Shepherd et al. (2012) noted that this source of uncertainty could reach up to 130 Gt/year (equivalent to 0.36 mm/year in terms of global sea level rise), which emphasizes why improvements on either aspect (IMC or GIA) would help make sea-level projections more accurate.

The aim of this study is to develop a methodology to combine GRACE data with high-resolution data sets to resolve mass variations of different origin with the highest possible spatial resolution. As a case study, we separate geophysical signals observed by GRACE over Antarctica by deriving the highest spatial resolution possible for GIA and IMC with the least possible noise level. For this, we simultaneously (i) improve the postprocessing of gravity data and (ii) consistently combine them with independent data featuring higher spatial resolution, such as altimetry and climate data. To achieve this, we refine the approach developed by Ran et al. (2017) by adapting the parameterization to the signal and use it in conjunction with the combination approach described in Gunter et al. (2014). This approach is hereafter termed the *dynamic patch approach* (DPA). A patch is a bounded region on Earth's surface with a constant mass layer. Akin to Baur and Sneeuw (2011), gravity disturbances at the satellite altitude are related in the functional model to the points on Earth's surface, but here the surface mass layer representation of Earth's gravitational field is used instead of a point-mass representation. This mass layer represents mass variations that occur over the patch, similar to mascons in, for example, Luthcke et al. (2013) and Watkins et al. (2015). The patches are defined based on geophysical boundaries, that is, by restricting ice-mass variations to the Antarctic Ice Sheet (AIS) by taking into account the grounding line position, identical to Chen et al. (2015). No destriping/filtering of GRACE data is required, because patches act as an inherent smoother on the data. That means that patch definition is essentially a regularization by parameterization and must be performed carefully (section 2.3). To help find an appropriate parameterization for the estimated GIA, use is made of independent GPS observations (section 3.1). The spatial resolution of the estimated IMC is determined using an ICESat-RACMO combination (section 3.1). To solve for GIA and IMC, weighted least-squares adjustment is applied while taking into account the full noise covariance matrix of monthly GRACE gravity models as well as the variances of other data sets involved in the combination without using any additional constraints. The key advantages of using the DPA is twofold: (1) it allows a consistent

combination of GRACE data with data that feature higher spatial resolution without yielding attenuation of their signal magnitude, and (2) it allows the GIA and IMC signals to be derived with high spatial resolution.

## 2. Methodology

### 2.1. Data Sets

Here we use unconstrained DMT2 (Delft Mass Transport model, release 2) GRACE monthly SH models including full noise covariance matrices complete to degree 120 (Farahani et al., 2016). Though our methodology can make use of any GRACE solution, we prefer DMT2 for its demonstrated quality and reliable noise covariance matrices as has been verified in Farahani et al. (2016). The latter is particularly important when combining data from GRACE with data from other observational techniques. As a complementary data set to gravimetry, the latest release of ICESat altimeter data (R634) is used. The ICESat mission period restricts the time span under investigation, from February 2003 to October 2009. Moreover, we only analyze linear trends derived over Antarctica, since ICESat was a campaign mission, and therefore, only linear trends can be detected reliably. It should however be noted that the full ICESat time series has sufficient sampling to adequately recover the long-term surface height trend. The ICESat processing details can be found in Felikson et al. (2017). Note that the methodology developed in this study is applicable to other temporal resolutions as long as auxiliary data are available, particularly when the assumption regarding the linearity of the GIA signal might not be valid (Barletta et al., 2018). To convert ICESat-derived height changes into mass, surface mass balance estimates from RACMO2.3 with accompanying firn densification model are utilized (Van Wessem et al., 2014). To define the pattern of estimated present-day GIA, GPS-derived uplift rates are used. The rates and corresponding uncertainties have been taken from Thomas et al. (2011), Groh et al. (2012), Argus et al. (2014), and Wolstencroft et al. (2015). If data at a GPS station were analyzed by more than one team, the uplift rates of the most recent study are used as they are expected to be reprocessed with the most accurate techniques. This yields 79 uplift rates for Antarctica. To use GPS-derived uplift rates for defining the pattern of estimated present-day GIA, two important assumptions are made. First, we assume that GIA evolves at constant rates over decades, meaning the time frames for the GPS trend analysis do not necessarily have to overlap with the time span under investigation, as long as elastic effects are considered. Elastic deformation is a response of the solid earth to contemporary surface load variations. Before using GPS observations to constrain the estimated GIA pattern, they need to be corrected for elastic deformation. To be consistent with data used in this analysis, elastic corrections are derived from the ICESat-RACMO combination, identical to the correction applied to the BREN site by Wolstencroft et al. (2015). The second assumption implies therefore that the linear trend based on the ICESat-RACMO combination sufficiently approximates the true variations in surface load over the time span considered.

### 2.2. Patch Approach

According to Ran et al. (2017), the gravity disturbances,  $\delta g$ , can be expressed in spherical coordinates for the point  $\mathbf{p}(r_i, \lambda_i, \varphi_i)$  at satellite altitude (500 km) and the source point  $\mathbf{p}'(r_{kj}, \lambda_{kj}, \varphi_{kj})$  as

$$\underbrace{\delta g_i}_y \approx \sum_{k=1}^K \underbrace{q_k}_{x_k} \underbrace{G \sum_{j=1}^{J_k} \Delta s_{kj} \frac{r_i - r_{kj} \cos \psi_{kj,i}}{(r_{kj}^2 + r_i^2 - 2r_{kj}r_i \cos \psi_{kj,i})^{3/2}}}_{A_{ik}} \quad (1)$$

with angular distance  $\cos \psi_{kj,i}$ , universal gravitational constant  $G$ , and surface density  $q_k$  of patch  $k$ . The weighted sum of  $\mathbf{p}'$ , where area elements  $\Delta s_{kj}$  serve as weights, is an approximation of the actual surface integral of the reciprocal distance contained in the computation of  $\delta g_i$  (detailed description is provided in supporting information Text S1).

The gravity disturbances can also be computed using the time-varying part of the SHs (Hofmann-Wellenhof & Moritz, 2006). Equation (1) together with  $\delta g_i$  computed using SHs represents the functional model for the patch approach where  $\delta g_i$  and  $q_k$  are stored in the observation and parameter vector, respectively. The design matrix  $A$  can be inferred from the right-hand side of equation (1) and contains geometrical information (e.g., data area at satellite altitude, area of interest on Earth's surface, and shape and size of patches) as it relates the source points (with index  $kj$ ) to the points at satellite altitude (with index  $i$ ). Close-loop simulations have been performed in Text S2 (Baur & Sneeuw, 2011; Colombo, 1981; Wahr et al., 1998) to demonstrate the capability of the patch approach to recover a synthesized (noise-free) gravitational signal.

### 2.3. Dynamic Patch Definition

Patch definition is essentially a regularization by parameterization and therefore crucial for the suggested approach. Since this case study focuses on separating GIA and IMC in Antarctica, we incorporate geophysical information about mass changes associated with these processes into the patch definition. While the RACMO and altimetry data sets provide reliable evidence for the heterogeneity of the surface processes over the AIS (Farahani et al., 2016), especially in the coastal areas, the spatial pattern of GIA signal over Antarctica is still not well understood. In most of East Antarctica (EA), GIA is believed to occur at large spatial scales (Whitehouse et al., 2012), while in WA, late Holocene IMC may dominate present-day GIA rates (Barletta et al., 2018; Gomez et al., 2018; Nield et al., 2014, 2016) that in combination with a thinner lithosphere yields shorter spatial scales of GIA patterns. For the patch-definition algorithm, this means that (1) it should be able to incorporate geophysical information about boundaries of the target regions, (2) patches of different sizes should easily be produced, and (3) no overlaps or gaps between the patches should occur.

An algorithm encompassing these features is the Voronoi decomposition (VD) applied on Fibonacci points (González, 2010). VD is the partitioning of the plane into convex polygons based on the distance to the generating points. We use Fibonacci points as generating points. By varying the distance between the Fibonacci points, the size of the produced patches varies. The larger the distance between the Fibonacci points, the more discontinuous is the pattern of the estimated signal. To derive the highest spatial maps as possible, a DPA is proposed. For this, patch boundaries are computed using a suite of different (dynamic) patch configurations yielding different estimates at the nodes of a predefined grid. The average of the different estimates at each node represents the final solution. To confirm the capability of the DPA to recover spatial pattern of a signal, a synthetic experiment is performed in Text S3 (Riva et al., 2009; Whitehouse et al., 2012).

### 2.4. Dynamic Patch Approach (DPA)

In this section, the approach presented in Gunter et al. (2014) is incorporated into the DPA. The key equation of Gunter et al. (2014) is simplified as

$$\dot{h}_{\text{rock}} = \frac{\dot{m}_{\text{GRACE}} - \dot{m}_{\text{surf}^*}}{d} \quad (2)$$

and relates the total mass change signal observed by GRACE,  $\dot{m}_{\text{GRACE}}$ , to the GIA-induced height changes,  $\dot{h}_{\text{rock}}$ , with

$$\dot{m}_{\text{surf}^*} = (\dot{m}_{\text{ICESat}} - \dot{m}_{\text{firn}}) \cdot \rho_{\alpha} + \dot{m}_{\text{firn}}, \quad (3)$$

representing the mass changes in the *surface* layer (ice + firn), and  $d = \rho_{\text{rock}} - \rho_{\alpha}$  is the denominator of their equation (3) containing the densities of rock and ice/firn. Therefore, *firn* implies all the processes modeled within the firn layer (Ligtenberg et al., 2011). Note that strictly speaking, the term *surface* mass changes can only be properly used after  $\dot{h}_{\text{rock}}$  is also subtracted from ICESat-derived height changes  $\dot{h}_{\text{ICESat}}$ . That is why a *surf*\* instead of *surf* label is used. From a computational point of view, the fact that ICESat theoretically observes the vertical rates related to GIA in addition to the surface processes is accounted for by including the density of ice/firn in the denominator of equation (2).

To help explain the algorithm of the DPA, the major steps are summarized in Figure 1 and described in Text S4 in more detail. The signal mainly associated with surface processes is subtracted from the total signal observed by GRACE following Gunter et al. (2014) but here in terms of gravity disturbances  $\delta g$  at the satellite altitude (Figure 1.3). To transfer as much information as possible of the signal into  $\delta g$  at 500-km altitude, the surface-layer patches are defined using a VD applied to a Fibonacci grid that is generated using 27-km distance between the Fibonacci points over AIS (VD(27) in Figure 1.3). The distance of 27 km is chosen because it corresponds to the spatial resolution of the RACMO data. These data have the lowest resolution in the computation of  $\dot{m}_{\text{surf}^*}$  in equation (3).

After subtracting  $\dot{m}_{\text{surf}^*}$  from the total GRACE signal at the satellite altitude, the remainder represents signal mainly associated with present-day GIA. GIA is estimated on the Earth's surface using the DPA (equation (1)). A VD is applied to parameterize signal. For this, the spacing of the Fibonacci grid varies between 100 and 700 km and 600 different grids are computed for each increment of 1 km (i.e., VD(100:1:700)). Since GIA might occur at large spatial scales, the boundaries for the VD extend to 400 km beyond the AIS. The weighted least-squares adjustment is then applied for each of the 600 patch configurations without using any additional constraints (Figure 1.5a). The full noise covariance matrix of GRACE product as well as the variances of other data sets involved in the combination (equation (3)) are formally propagated. The standard deviations described in Gunter et al. (2014) are utilized for individual components of equation (3).

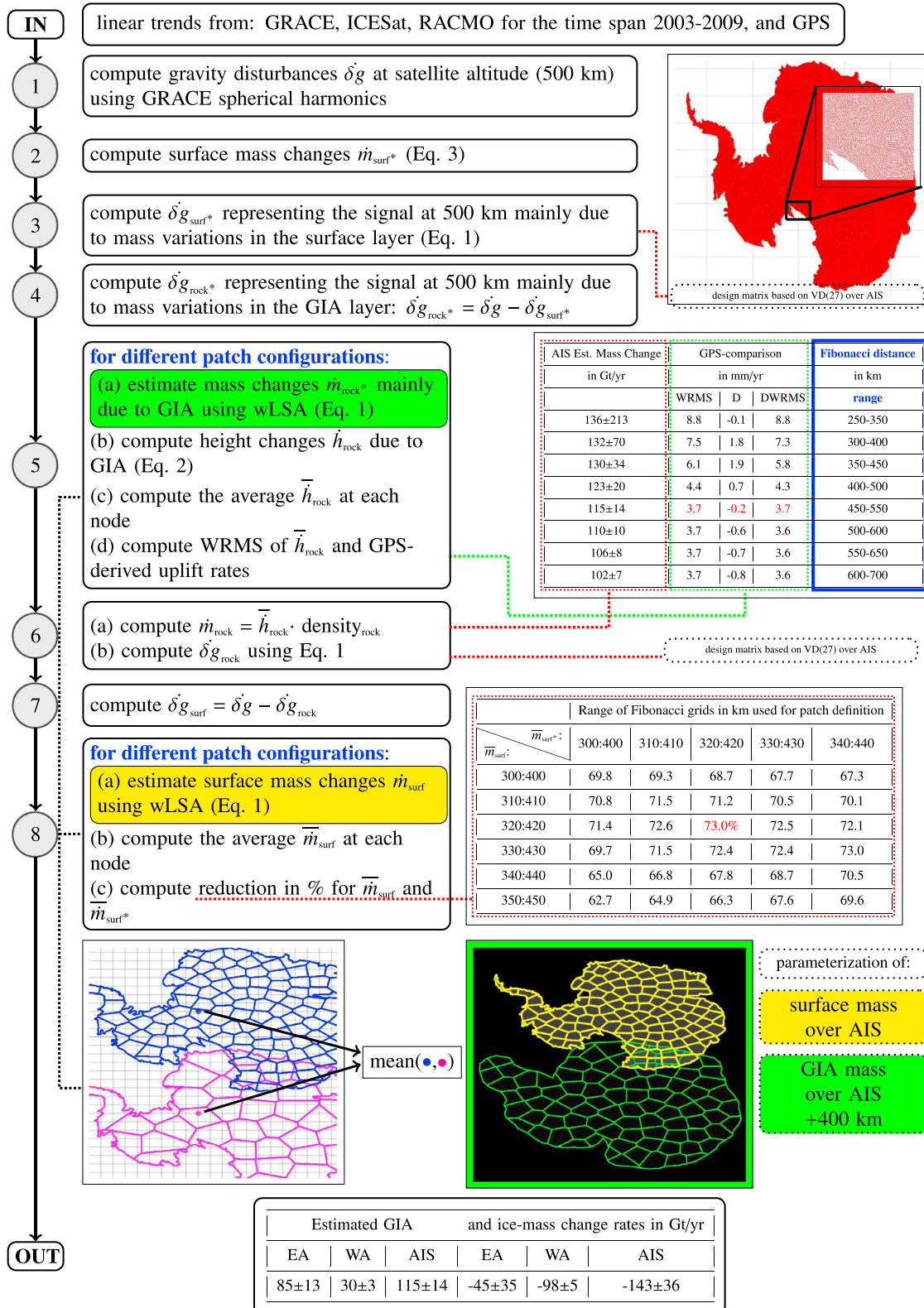


**Figure 1.** Flow diagram to summarize the major steps of the dynamic patch approach. wLSA = weighted least-squares adjustment;  $VD_{27}$  = Voronoi decomposition based on Fibonacci points with 27-km distance between them; WRMS = weighted root-mean-square of the residuals; DWRMS = for bias D corrected WRMS; GIA = glacial isostatic adjustment; GRACE = Gravity Recovery and Climate Experiment; ICESat = Ice Cloud and land Elevation Satellite; RACMO = Regional Atmospheric Climate Model; AIS = Antarctic Ice Sheet; EA = East Antarctica; WA = West Antarctica.

To get height changes  $\dot{h}_{\text{rock}}$  associated with GIA, the estimated mass changes are divided by the corresponding  $d$  according to equation (2) (Figure 1.5b). To find a preferred GIA solution, we examined how the spatial pattern and the magnitude of the estimates evolves over different patch configurations. For this, the produced range of solutions was subdivided using a sliding window width of 100 km and a sliding increment of 50 km, for example, 100–200, 150–250 km, and so on, yielding 11 GIA estimates for VD(100:1:700). Only the results using VD(250:1:700) are considered further (Figure 1.6a and Figure S5), as the signal content of the results based on VD(100:1:250) is considerably lower than their noise content. The sliding window width of 100 km was identified based on synthetic experiments. The 50-km-wide sliding increment is used, because it leads to estimates that are sufficiently different but still within  $1\sigma$  range of subsequent uncertainties (Figure 1.6a). To get a continuous pattern of the estimated signal, a solution is generated by averaging 100 different solutions, which were estimated using 100 different patch configurations (Figure 1.5c). The averages are computed at each node of the cubature formula defined by the 0.05-degree Gauss-Neumann grid (Sneeuw, 1994). The nodes of the cubature formula are used to numerically compute the surface integral of the reciprocal distance contained in the functional model in equation (1). From the eight resulting GIA solutions, we compare the estimated vertical rates at the GPS station sites with the corresponding observed (elastic-corrected) GPS vertical rates to determine the preferred VD parameterization. The agreement is analyzed according to Wolsentcroft et al. (2015) in terms of the weighted root-mean-square of the residuals (WRMS) and bias-corrected WRMS (DWRMS) as can be seen in Figure 1.5d.

The preferred GIA solution is multiplied by the density of rock (Figure 1.6a). The chosen rock density values and corresponding uncertainties are the same as by Gunter et al. (2014). The resulting empirical GIA mass change rates are then subtracted from the total signal observed by GRACE in terms of gravity disturbances (Figures 1.6b and 1.7). The remainder represents signal due to IMC (ice and firn) and is estimated on Earth's surface again using the DPA. Similarly to defining patches for the GIA layer, different Fibonacci grids spanning the range between 100 and 700 km are used to define patches for the surface layer, but this time, the VD is performed over the grounded portion of the ice sheet only (Figure 1). This is an extremely advantageous feature of the DPA, since mass variations associated with surface processes can be localized over the ice sheet instead of leaking into the ocean, assuming the GIA is estimated correctly.

Just as for the GIA layer, IMC estimates for the range of VD(100:1:700) are computed using a sliding window width of 100 km and a sliding increment of 50 km yielding 11  $\bar{m}_{\text{surf}}$  estimates (Figures 1.8a, 1.8b, and S6). To help decide which range of patches is the preferred one for estimating IMC, ICESat-RACMO combination is used ( $\dot{m}_{\text{surf}}^*$  from equation (3)) since it provides a good reference of the spatial pattern of surface processes (Farahani et al., 2016). Before comparing differently parameterized IMC estimates  $\bar{m}_{\text{surf}}$  with  $\dot{m}_{\text{surf}}^*$ , the latter undergoes a similar procedure as GRACE-derived observations to ensure a fair comparison. That means that gravity disturbances computed at satellite altitude using  $\dot{m}_{\text{surf}}^*$  are used as pseudo-observations to estimate  $\bar{m}_{\text{surf}}^*$ . The  $\bar{m}_{\text{surf}}^*$  is parameterized in the same way as IMC estimates derived from the full combination (i.e., GRACE-ICESat-RACMO) yielding 11  $\bar{m}_{\text{surf}}^*$  estimates. The IMC estimate with the closest agreement to  $\bar{m}_{\text{surf}}^*$  is regarded as the preferred one (Figure 1.8c). As a criterion for similarity, RMS reduction in percent is used following Tesmer et al. (2011) and described in Text S6.

When using the suggested DPA, both GIA and IMC are parameterized using different geophysical boundaries and different patch configurations without estimating the total GRACE mass change on Earth's surface. A calibration over a known low-precipitation zone (LPZ) is done following Gunter et al. (2014) by computing and subtracting a LPZ bias from the estimated GIA and IMC rates before integrating them over the AIS.

### 3. Results and Discussion

#### 3.1. GIA and IMC Estimates

The geographical plots of the results along with the corresponding uncertainties are shown in Figures 2a–2d. The GIA-estimate using VD(450:1:550) shown in Figure 2a has the lowest WRMS and DWRMS of 3.7 mm/year at the GPS sites compared to other GIA parameterizations (Figure 1.5d). For larger patches, WRMS and corresponding DWRMS are not changing significantly. Note that when using VD(450:1:550) to parameterize GIA, the systematic bias  $D$  between estimated GIA rates and those observed from the GPS stations is one of the smallest (in an absolute sense) in Figure 1.5d.

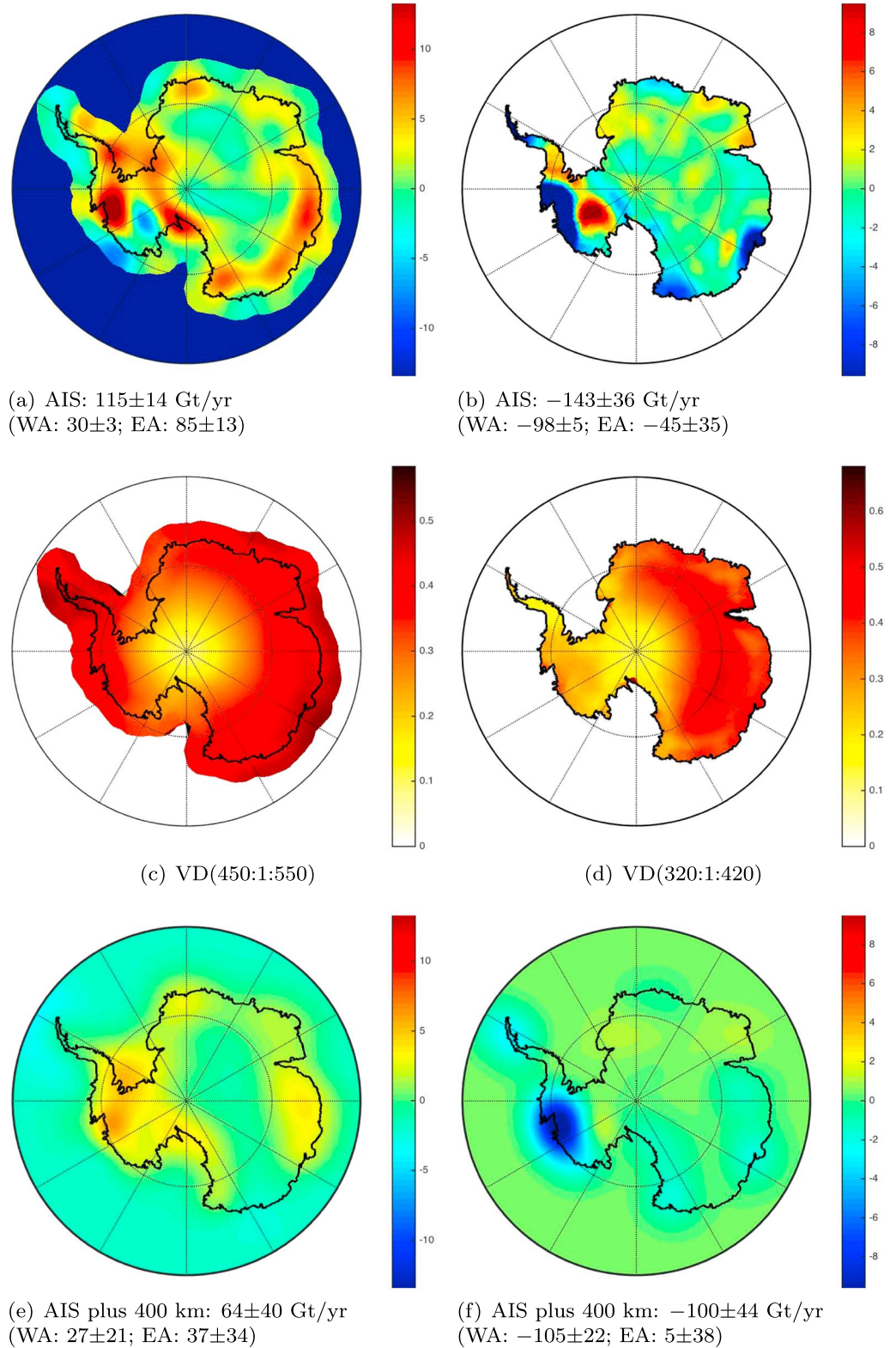


**Figure 2.** Estimates (a and b) and uncertainties (c and d) for the estimated glacial isostatic adjustment rates (a and c) in millimeter per year and ice-mass change rates (b and d) in centimeter per year Equivalent Water Heights. Glacial isostatic adjustment (e) and ice-mass change (f) estimated by Gunter et al. (2014). AIS = Antarctic Ice Sheet; WA = West Antarctica; EA = East Antarctica; VD = Voronoi decomposition.

The preferred IMC estimate using VD(320:1:420) is shown in Figure 2b. To refine the IMC estimates, a smaller sliding increment of 10 km was used to find the preferred parameterization of 320–420 km for the Fibonacci grids (Figure 1.8c), which yielded the maximum value of 73% for the reduction in percent for  $\overline{m}_{\text{surf}^*}$  and  $\overline{m}_{\text{surf}}$ .

### 3.2. Discussion

To examine any differences in the GIA and IMC estimates from the DPA methodology with those from earlier studies, we first compared the results with a representative case from Gunter et al. (2014) based on their CSR RL05 DDK5 GRACE variant (named G14 hereafter). These results are shown in Figures 2e and 2f, for GIA and IMC, respectively. Comparing Figures 2a and 2b with 2e and 2f, the enhanced spatial resolution due to the modified methodology is clearly evident. Although over the AIS integrated mass changes agree within  $1\sigma$  range, there are substantial differences in EA. One possible reason for these differences is the updated RACMO2.3 data set that simulates considerably wetter conditions in the interior of EA than its predecessor RACMO2.1 used in G14 (Van Wessem et al., 2014). The disagreement is reflected in the GIA-induced mass estimates over EA which increase compared to earlier work from  $37 \pm 34$  to  $85 \pm 13$  Gt/year. The corresponding IMC in EA are difficult to compare, as previous estimates barely contain any spatial details (Figures 2b and 2f). Moreover, both estimates are not statistically significant because of relatively low signal-to-noise ratio over a large area.

For WA, the mass change estimates are robust against different data and modified methodology, showing a very good agreement between both mass changes related to GIA and surface processes (Figures 2a, 2b, 2e, and 2f). The high-resolution spatial map of the updated GIA estimate (Figure 2a) shows the highest uplift rates in the Amundsen Sea Embayment (ASE). The high GIA uplift rates in this region were first suggested by Groh et al. (2012) with its spatial map first being shown in Gunter et al. (2014). The genuineness of a GIA uplift in ASE was then confirmed by Martín-Español, Zammit-Mangion, et al. (2016) once they constrained spatial wavelength of GIA using forward models. Sasgen et al. (2017), identical to Martín-Español, Zammit-Mangion, et al. (2016), derived strong GIA signal in ASE by combining complementary geodetic observations when considering the weak Earth structure in the determination of the viscoelastic response functions they utilized. The pronounced GIA-induced uplift is supported by recent GIA models that consider late Holocene IMC which seem to dominate present-day GIA rates in regions that have a thinner lithosphere and a lower mantle viscosity (Barletta et al., 2018; Gomez et al., 2018). According to Barletta et al. (2018), the forward-modeled GIA correction over the Antarctic basins 21 and 22 (Zwally et al., 2012) for the GRACE-derived mass loss is between 13.5 and 19.4 Gt/year. Our estimate of  $17.8 \pm 0.7$  Gt/year compares well with the forward-modeled GIA. We note that it is remarkable that forward-modeled and empirically estimated GIA solutions start to converge in this region, which is extremely important in light of current discussions regarding the future of the AIS and its contribution to the sea-level rise.

Entirely new in our data-driven GIA solution is the subsidence of maximum  $-8$  mm/year (Figure 2a) in the proximity of Kamb Ice Stream. Through forward modeling, Nield et al. (2016) have demonstrated that a significant present-day GIA signal might occur in response to the Late Holocene ice changes related to stagnation and reactivation of ice streams in this area. Although heavily depending on the regional upper mantle viscosity, Nield et al. (2016) have shown that GIA model-predicted rates in this region can reach up to  $-17$  mm/year. Their study supports, therefore, our data-driven GIA-induced subsidence in WA. A negative GIA-induced signal is also predicted from a coupled model with the 3-D Earth model by Gomez et al. (2018) when ice cover changes over the last 3 kyr are considered. The error analysis (Figure 2c) confirms the statistical significance of the estimates (at the 95% level of confidence). This indicates that the proposed DPA allows the complex spatial pattern of the present-day GIA-induced vertical deformation to be detected.

Comparing the estimated GIA-induced apparent mass trend with other recent studies that are largely independent of forward models yields no consensus. Martín-Español, Zammit-Mangion, et al. (2016) derived GIA-induced mass changes of  $55 \pm 8$  Gt/year over the AIS along with IMC of  $-42 \pm 24$  Gt/year for the same time period considered here. Although, their spatially varying constraints led to a spatial GIA pattern in ASE (Figure 10 in Martín-Español, Zammit-Mangion, et al., 2016) that is similar to our estimated GIA, the area-integrated mass changes differ significantly for both GIA and IMC. Nevertheless, both results suggest ice-mass loss over the AIS. This is not the case for the study by Zwally et al. (2015) who derived an ice-mass increase over AIS for a similar time period (2003–2008) of  $82 \pm 25$  Gt/year. The inconsistencies between the recent studies emphasize the need for further research.

#### 4. Conclusions

Unconstrained GRACE time-variable gravity fields with their full covariance information have been used together with ICESat, RACMO2.3, and GPS displacement data to derive high-resolution spatial maps for GIA and IMC over Antarctica. For this, a DPA has been developed that removes correlated noise in GRACE data, since the approach acts as a statistical filter that uses (full) variance-covariance matrix and does not require any a priori information regarding the magnitude of the estimated signal. The DPA also allows a consistent combination of GRACE data with other complementary data that feature higher spatial resolution (i.e., ICESat altimetry and RACMO climate data) without yielding attenuation of their signal magnitude. While using different patch configurations, the proposed approach incorporates geophysical knowledge about boundaries of the parameterized signal avoiding spatial leakage between the land and adjacent ocean. It also allows complex spatial patterns, if they exist, to be detected.

A range of different solutions based on different patch configurations was estimated for signals associated with GIA and IMC over Antarctica. Independent GPS observations helped decide that the range of patches based on 450–550-km Fibonacci grids is the most suitable for parameterizing Antarctic GIA signal. The most suitable parameterization for IMC was determined to be the range of patches based on 320–420-km Fibonacci grids. This parameterization yields the best fit between the estimated IMC and the ICESat-RACMO combination. As a result, the empirically derived GIA and IMC signals exhibit unprecedented high spatial resolution. For the first time, data-driven GIA contains a pronounced subsidence in the proximity of the Kamb Ice Stream in response to the Late Holocene ice changes. The developed method recovers statistically significant high-resolution maps of mass loss for WA ( $-98 \pm 5$  Gt/year) and the entire AIS ( $-143 \pm 36$  Gt/year) for the ICESat mission period. The fact that the data used in this study are 7-years old does not influence the derived GIA rates which are assumed to be time invariant over very short geologic time frames. When analyzing time periods longer than a decade, time-varying GIA can be derived using the suggested approach in places like WA, as long as auxiliary data are available with a suitable temporal resolution. We derived the IMC for the ICESat time span to demonstrate the capability of the proposed approach to recover high-resolution spatial pattern. The developed method can be applied on data derived from, for example, the upcoming ICESat-2 and GRACE Follow-On missions and in any other application which involves GRACE data and any other geodetic data. Moreover, our empirical estimates can help validate the next generation of numerical models that attempt to take into account the lateral heterogeneities in Earth structure (van der Wal et al., 2015).

#### Acknowledgments

RACMO data were provided by J. Lenarts, S. Ligtenberg, and M. van den Broeke from Utrecht University. P. Ditmar and H. Hashemi Farahani, from Delft University of Technology, provided DMT2 solutions with full noise covariance matrices. ICESat trends were provided by B. Gunter. This research was financially supported by the Netherlands Organization for Scientific Research as part of the New Netherlands Polar Programme. The estimated GIA and ice-mass change rates with corresponding uncertainties are available at <https://doi.org/10.4121/uuid:2b189219-5597-4c87-8d91-0cbf43d43325>.

#### References

- Argus, D. F., Peltier, W., Drummond, R., & Moore, A. W. (2014). The Antarctica component of postglacial rebound model ICE-6G\_C (VM5a) based on GPS positioning, exposure age dating of ice thicknesses, and relative sea level histories. *Geophysical Journal International*, *198*(1), 537–563.
- Barletta, V. R., Bevis, M., Smith, B. E., Wilson, T., Brown, A., Bordoni, A., et al. (2018). Observed rapid bedrock uplift in Amundsen Sea Embayment promotes ice-sheet stability. *Science*, *360*(6395), 1335–1339.
- Baur, O., & Sneeuw, N. (2011). Assessing Greenland ice mass loss by means of point-mass modeling: A viable methodology. *Journal of Geodesy*, *85*(9), 607–615.
- Chen, J., Wilson, C., Li, J., & Zhang, Z. (2015). Reducing leakage error in GRACE-observed long-term ice mass change: A case study in West Antarctica. *Journal of Geodesy*, *89*(9), 925–940.
- Colombo, O. L. (1981). Numerical methods for harmonic analysis on the sphere. Department of Geodetic Science, The Ohio State University.
- Farahani, H. H., Ditmar, P., Inácio, P., Didova, O., Gunter, B., Klees, R., et al. (2016). A high resolution model of linear trend in mass variations from DMT-2: Added value of accounting for coloured noise in GRACE data. *Journal of Geodynamics*, *103*, 12–25.
- Felikson, D., Urban, T. J., Gunter, B. C., Pie, N., Pritchard, H. D., Harpold, R., & Schutz, B. E. (2017). Comparison of elevation change detection methods from ICESat altimetry over the Greenland ice sheet. *IEEE Transactions on Geoscience and Remote Sensing*, *55*(10), 5494–5505.
- Gomez, N., Latychev, K., & Pollard, D. (2018). A coupled ice sheet–sea level model incorporating 3D earth structure: Variations in Antarctica during the last deglacial retreat. *Journal of Climate*, *31*(10), 4041–4054.
- González, Á. (2010). Measurement of areas on a sphere using Fibonacci and latitude–longitude lattices. *Mathematical Geosciences*, *42*(1), 49–64.
- Groh, A., Ewert, H., Scheinert, M., Fritsche, M., Rülke, A., Richter, A., et al. (2012). An investigation of glacial isostatic adjustment over the Amundsen Sea Sector, West Antarctica. *Global and Planetary Change*, *98–99*(0), 45–53. <https://doi.org/10.1016/j.gloplacha.2012.08.001>
- Gunter, B., Didova, O., Riva, R., Ligtenberg, S., Lenaerts, J., King, M., et al. (2014). Empirical estimation of present-day antarctic glacial isostatic adjustment and ice mass change. *Cryosphere*, *8*(2), 743–760.
- Hofmann-Wellenhof, B., & Moritz, H. (2006). *Physical geodesy*. Vienne: Springer Science & Business Media.
- Humphrey, V., Gudmundsson, L., & Seneviratne, S. I. (2017). A global reconstruction of climate-driven subdecadal water storage variability. *Geophysical Research Letters*, *44*, 2300–2309. <https://doi.org/10.1002/2017GL072564>
- Klees, R., Revtova, E. A., Gunter, B. C., Ditmar, P., Oudman, E., Winsemius, H. C., & Savenije, H. H. G. (2008). The design of an optimal filter for monthly GRACE gravity models. *Geophysical Journal International*, *175*(2), 417–432. <https://doi.org/10.1111/j.1365-246X.2008.03922.x>
- Kusche, J. (2007). Approximate decorrelation and non-isotropic smoothing of time-variable GRACE-type gravity field models. *Journal of Geodesy*, *81*, 733–749. <https://doi.org/10.1007/s00190-007-0143-3>

- Ligtenberg, S. R. M., Helsen, M. M., & van den Broeke, M. R. (2011). An improved semi-empirical model for the densification of Antarctic firn. *The Cryosphere*, 5(4), 809–819. <https://doi.org/10.5194/tc-5-809-2011>
- Luthcke, S. B., Sabaka, T., Loomis, B., Arendt, A., McCarthy, J., & Camp, J. (2013). Antarctica, Greenland and gulf of Alaska land-ice evolution from an iterated GRACE global mascon solution. *Journal of Glaciology*, 59(216), 613–631.
- Martin-Español, A., King, M. A., Zammit-Mangion, A., Andrews, S. B., Moore, P., & Bamber, J. L. (2016). An assessment of forward and inverse GIA solutions for Antarctica. *Journal of Geophysical Research: Solid Earth*, 121, 6947–6965. <https://doi.org/10.1002/2016JB013154>
- Martin-Español, A., Zammit-Mangion, A., Clarke, P. J., Flament, T., Helm, V., King, M. A., et al. (2016). Spatial and temporal Antarctic ice sheet mass trends, glacio-isostatic adjustment, and surface processes from a joint inversion of satellite altimeter, gravity and GPS data. *Journal of Geophysical Research: Earth Surface*, 121, 182–200.
- Nield, G. A., Barletta, V. R., Bordoni, A., King, M. A., Whitehouse, P. L., Clarke, P. J., et al. (2014). Rapid bedrock uplift in the Antarctic Peninsula explained by viscoelastic response to recent ice unloading. *Earth and Planetary Science Letters*, 397, 32–41.
- Nield, G. A., Whitehouse, P. L., King, M. A., & Clarke, P. J. (2016). Glacial isostatic adjustment in response to changing Late Holocene behaviour of ice streams on the Siple Coast, West Antarctica. *Geophysical Journal International*, 205(1), 1–21.
- Ran, J., Ditmar, P., Klees, R., & Farahani, H. (2017). Statistically optimal estimation of Greenland ice sheet mass variations from GRACE monthly solutions using an improved mascon approach. *Journal of Geodesy*, 92, 1–21.
- Riva, R. E. M., Gunter, B. C., Urban, T. J., Vermeersen, B. L. A., Lindenberg, R. C., Helsen, M. M., et al. (2009). Glacial isostatic adjustment over Antarctica from combined ICESat and GRACE satellite data. *Earth and Planetary Science Letters*, 288, 516–523. <https://doi.org/10.1016/j.epsl.2009.10.013>
- Sasgen, I., Martin-Español, A., Horvath, A., Klemann, V., Petrie, E. J., Wouters, B., et al. (2017). Joint inversion estimate of regional glacial isostatic adjustment in Antarctica considering a lateral varying earth structure (ESA STSE Project REGINA). *Geophysical Journal International*, 211(3), 1534–1553.
- Shepherd, A., Ivins, E. R., Geruo, A., Barletta, V. R., Bentley, M. J., Bettadpur, S., et al. (2012). A reconciled estimate of ice-sheet mass balance. *Science*, 338(6111), 1183–1189.
- Siemes, C., Ditmar, P., Riva, R., Slobbe, D., Liu, X., & Farahani, H. (2013). Estimation of mass change trends in the Earth's system on the basis of GRACE satellite data, with application to Greenland. *Journal of Geodesy*, 87, 69–87. <https://doi.org/10.1007/s00190-012-0580-5>
- Sneeuw, N. (1994). Global spherical harmonic analysis by least-squares and numerical quadrature methods in historical perspective. *Geophysical Journal International*, 118(3), 707–716.
- Swenson, S., & Wahr, J. (2006). Post-processing removal of correlated errors in GRACE data. *Geophysical Research Letters*, 33, L08402. <https://doi.org/10.1029/2005GL025285>
- Teixeira Encarnação, J. (2015). Next-generation satellite gravimetry for measuring mass transport in the Earth system (PhD thesis), TU Delft, Delft University of Technology.
- Tesmer, V., Steigenberger, P., van Dam, T., & Mayer-Gürr, T. (2011). Vertical deformations from homogeneously processed grace and global GPS long-term series. *Journal of Geodesy*, 85, 291–310.
- Thomas, I. D., King, M. A., Bentley, M. J., Whitehouse, P. L., Penna, N. T., Williams, S. D. P., et al. (2011). Widespread low rates of Antarctic glacial isostatic adjustment revealed by GPS observations. *Geophysical Research Letters*, 38, L22302. <https://doi.org/10.1029/2011GL049277>
- Van Wessem, J., Reijmer, C., Morlighem, M., Mougnot, J., Rignot, E., Medley, B., et al. (2014). Improved representation of East Antarctic surface mass balance in a regional atmospheric climate model. *Journal of Glaciology*, 60(222), 761–770.
- van der Wal, W., Whitehouse, P. L., & Schrama, E. (2015). Effect of GIA models with 3D composite mantle viscosity on GRACE mass balance estimates for Antarctica. *Earth and Planetary Science Letters*, 414, 134–143.
- Wahr, J., Molenaar, M., & Bryan, F. (1998). Time variability of the Earth's gravity field: Hydrological and oceanic effects and their possible detection using GRACE. *Journal of Geophysical Research*, 103(B12), 30,205–30,229.
- Watkins, M. M., Wiese, D. N., Yuan, D.-N., Boening, C., & Landerer, F. W. (2015). Improved methods for observing Earth's time variable mass distribution with GRACE using spherical cap mascons. *Journal of Geophysical Research: Solid Earth*, 120, 2648–2671. <https://doi.org/10.1002/2014JB011547>
- Whitehouse, P. L., Bentley, M. J., Milne, G. A., King, M. A., & Thomas, I. D. (2012). A new glacial isostatic adjustment model for Antarctica: Calibrated and tested using observations of relative sea-level change and present-day uplift rates. *Geophysical Journal International*, 190(3), 1464–1482. <https://doi.org/10.1111/j.1365-246X.2012.05557.x>
- Wolstencroft, M., King, M. A., Whitehouse, P. L., Bentley, M. J., Nield, G. A., King, E. C., et al. (2015). Uplift rates from a new high-density GPS network in Palmer Land indicate significant Late Holocene ice loss in the Southwestern Weddell Sea. *Geophysical Journal International*, 203(1), 737–754.
- Wong, L., Buechler, G., Downs, W., Sjogren, W., Muller, P., & Gottlieb, P. (1971). A surface-layer representation of the lunar gravitational field. *Journal of Geophysical Research*, 76(26), 6220–6236.
- Zwally, H. J., Giovinetto, M. B., Beckley, M. A., & Saba, J. L. (2012). *Antarctic and Greenland drainage systems*. GSFC Cryospheric Sciences Laboratory. Retrieved from [http://icesat4.gsfc.nasa.gov/cryo\\_data/ant\\_grn\\_drainage\\_systems.php](http://icesat4.gsfc.nasa.gov/cryo_data/ant_grn_drainage_systems.php)
- Zwally, H. J., Li, J., Robbins, J. W., Saba, J. L., Yi, D., & Brenner, A. C. (2015). Mass gains of the Antarctic ice sheet exceed losses. *Journal of Glaciology*, 61(230), 1019–1036.

## Erratum

In the originally published version of this article, there was an error in the published affiliations of Riccardo Riva and Roland Klees. Both authors are affiliated with Department of Geoscience and Remote Sensing, Delft University of Technology, Delft, The Netherlands. These errors have since been corrected, and this version may be considered the authoritative version of record.